Gradient Dynamics of Attention: How Cross-Entropy Sculpts Bayesian Manifolds

Paper II of the Bayesian Attention Trilogy

NAMAN AGARWAL*, Dream Sports, USA
SIDDHARTHA R. DALAL, Columbia University, USA
VISHAL MISRA, Columbia University, USA

Transformers empirically perform precise probabilistic reasoning in carefully constructed "Bayesian wind tunnels" and in large-scale language models, yet the mechanisms by which gradient-based learning creates the required internal geometry remain opaque. We provide a systematic first-order analysis of how cross-entropy training reshapes attention scores and value vectors in a transformer attention head. Our core result is an *advantage-based routing law* for attention scores,

$$\frac{\partial L}{\partial s_{ij}} = \alpha_{ij}\big(b_{ij} - \mathbb{E}_{\alpha_i}[b]\big), \qquad b_{ij} := u_i^\top v_j,$$

coupled with a *responsibility-weighted update* for values v_j,

$$\Delta v_j = -\eta \sum_i \alpha_{ij} u_i,$$

where u_i is the upstream gradient at position i and α_{ij} are attention weights. These equations induce a positive feedback loop in which routing and content specialize together: queries route more strongly to values that are above-average for their error signal, and those values are pulled toward the queries that use them. We show that this coupled specialization behaves like a two-timescale EM procedure: attention weights implement an E-step (soft responsibilities), while values implement an M-step (responsibility-weighted prototype updates), with queries and keys adjusting the hypothesis frame. Through controlled simulations, including a sticky Markov-chain task where we compare a closed-form EM-style update to standard SGD, we demonstrate that the same gradient dynamics that minimize cross-entropy also sculpt the low-dimensional manifolds identified in our companion work as implementing Bayesian inference. Further, in EM versus SGD comparison, EM converges much faster, and predictive entropy for both is close to minimum Bayesian entropy. This yields a unified picture in which optimization (gradient flow) gives rise to geometry (Bayesian manifolds), which in turn supports function (in-context probabilistic reasoning).

1 Introduction

Transformers have become the dominant architecture for sequence modeling, yet we still lack a mechanistic understanding of *how* gradient descent sculpts their internal representations. Recent work has shown that in controlled "Bayesian wind tunnels" a small transformer can reproduce analytic posteriors exactly, with keys forming orthogonal hypothesis axes, queries implementing progressive belief updates, and values unfurling along one-dimensional manifolds parameterized by posterior entropy [1]. Our companion scaling paper extends this picture to production-scale models, showing similar geometric signatures in Pythia, Phi-2, and LLaMA.

These findings raise a natural question: *Why does plain cross-entropy training produce the very geometric structures required for Bayesian inference?* Understanding this requires moving from static geometry to *gradient dynamics*: how do attention scores, queries, keys, and values co-evolve during optimization?

---

*Currently at Google DeepMind. Work performed while at Dream Sports.

This paper provides a mechanistic account. We analyze a single-head attention block trained with cross-entropy and derive all first-order gradients with respect to scores s_{ij}, queries q_i, keys k_j, and values v_j. We then interpret the resulting gradient flows and connect them to the Bayesian manifolds observed empirically.

1.1 Contributions

Our main contributions are:

(1) **Complete first-order analysis of attention gradients.** We derive closed-form expressions for $\partial L/\partial s_{ij}$, $\partial L/\partial q_i$, $\partial L/\partial k_j$, and $\partial L/\partial v_j$ under cross-entropy loss, in a form that makes their geometric meaning transparent.

(2) **Advantage-based routing law.** We show that score gradients satisfy

$$\frac{\partial L}{\partial s_{ij}} = \alpha_{ij}\big(b_{ij} - \mathbb{E}_{\alpha_i}[b]\big),$$

where $b_{ij} = u_i^\top v_j$ is a compatibility term. Attention scores increase for positions whose compatibility exceeds the current attention-weighted mean, and decrease otherwise.

(3) **Responsibility-weighted value updates and specialization.** Values evolve according to

$$\Delta v_j = -\eta \sum_i \alpha_{ij} u_i,$$

a responsibility-weighted average of upstream gradients. This induces a positive feedback loop: queries route to values that help them; those values move toward their users, reinforcing routing and creating specialization.

(4) **Two-timescale EM interpretation.** We show that these dynamics implement an implicit EM-like algorithm: attention weights act as soft responsibilities (E-step), values as prototypes updated under those responsibilities (M-step), and queries/keys as parameters of the latent assignment model. Attention often stabilizes early, while values continue to refine—a frame–precision dissociation that matches our empirical observations in wind tunnels and large models.

(5) **Toy experiments and EM vs. SGD comparison.** In synthetic tasks, including a sticky Markov-chain sequence, we compare a closed-form EM-style update induced by our gradient analysis to standard SGD. EM reaches low loss, high accuracy, and sharp predictive entropy significantly faster; SGD converges to similar solutions but with slower and more diffuse routing. PCA visualizations of value trajectories reveal emergent low-dimensional manifolds.

Taken together with [1], our results provide a unified story:

$$\textit{Gradient descent} \implies \textit{Bayesian manifolds} \implies \textit{In-context inference.}$$

Clarification on "Bayesian inference." Throughout this paper, "Bayesian inference" refers to the *Bayesian posterior predictive over latent task variables*—not a posterior over network weights. We show that cross-entropy training sculpts geometry that implements Bayesian filtering over in-context hypotheses, not Bayesian weight uncertainty.

2 Setup and Notation

We analyze a single attention head operating on a sequence of length T. Indices i, j, k run from 1 to T unless stated otherwise.

2.1 Forward Pass

At each position j we have an input embedding $x_j \in \mathbb{R}^{d_x}$. Linear projections produce queries, keys, and values:

$$q_i = W_Q x_i \in \mathbb{R}^{d_k}, \tag{1}$$

$$k_j = W_K x_j \in \mathbb{R}^{d_k}, \tag{2}$$

$$v_j = W_V x_j \in \mathbb{R}^{d_v}. \tag{3}$$

Attention scores, weights, and context vectors are:

$$s_{ij} = \frac{q_i^\top k_j}{\sqrt{d_k}}, \tag{4}$$

$$\alpha_{ij} = \frac{\exp(s_{ij})}{\sum_r \exp(s_{ir})}, \tag{5}$$

$$g_i = \sum_{j=1}^{T} \alpha_{ij} v_j \in \mathbb{R}^{d_v}. \tag{6}$$

The output of the head is passed through an output projection to logits:

$$\ell_i = W_O g_i + b \in \mathbb{R}^C, \tag{7}$$

$$p_i = \text{softmax}(\ell_i), \tag{8}$$

and we train with cross-entropy loss

$$L = -\sum_{i=1}^{T} \log p_{i,y_i}, \tag{9}$$

where y_i is the target class at position i.

2.2 Auxiliary Quantities

For compactness we define:

$$u_i := \frac{\partial L}{\partial g_i} = W_O^\top (p_i - e_{y_i}) \in \mathbb{R}^{d_v}, \tag{10}$$

$$b_{ij} := u_i^\top v_j \in \mathbb{R}, \tag{11}$$

$$\mathbb{E}_{\alpha_i}[b] := \sum_{j=1}^{T} \alpha_{ij} b_{ij}. \tag{12}$$

Here u_i is the upstream gradient at position i, indicating how g_i should move to reduce the loss. The scalar b_{ij} measures compatibility between the error signal u_i and value v_j, and $\mathbb{E}_{\alpha_i}[b]$ is the attention-weighted mean compatibility for query i.

3 First-Order Gradient Derivations

We now derive all relevant gradients without skipping steps, focusing on forms that reveal their geometric meaning.

3.1   Output Gradient

For each i, the cross-entropy gradient with respect to logits is

$$\frac{\partial L}{\partial \ell_i} = p_i - e_{y_i}. \tag{13}$$

This propagates back to the context g_i as

$$u_i := \frac{\partial L}{\partial g_i} = W_O^{\top}(p_i - e_{y_i}). \tag{14}$$

Intuitively, $-u_i$ is the direction in value space along which moving g_i would increase the logit of the correct token and decrease loss.

3.2   Gradient with Respect to Values

Since $g_i = \sum_j \alpha_{ij} v_j$, we have

$$\frac{\partial L}{\partial v_j} = \sum_{i=1}^{T} \frac{\partial L}{\partial g_i} \frac{\partial g_i}{\partial v_j} = \sum_{i=1}^{T} u_i \alpha_{ij}. \tag{15}$$

Thus

$$\boxed{\frac{\partial L}{\partial v_j} = \sum_{i=1}^{T} \alpha_{ij}\, u_i.} \tag{16}$$

Geometrically, v_j is pulled toward an attention-weighted average of upstream error vectors from all queries that use it.

3.3   Gradient with Respect to Attention Weights

Because g_i depends linearly on α_{ij}, we obtain

$$\frac{\partial L}{\partial \alpha_{ij}} = \left(\frac{\partial L}{\partial g_i}\right)^{\top} \frac{\partial g_i}{\partial \alpha_{ij}} = u_i^{\top} v_j = b_{ij}. \tag{17}$$

The scalar $b_{ij} = u_i^{\top} v_j$ measures the instantaneous compatibility between the upstream gradient u_i and value vector v_j. Since $\partial L/\partial \alpha_{ij} = b_{ij}$, increasing α_{ij} increases the loss when $b_{ij} > 0$ and decreases the loss when $b_{ij} < 0$. Thus, $-b_{ij}$ represents the immediate marginal benefit (in loss reduction) of allocating additional attention mass to position j for query i.

3.4   Gradient with Respect to Scores

For fixed i, the softmax Jacobian is

$$\frac{\partial \alpha_{ij}}{\partial s_{ik}} = \alpha_{ij}(\delta_{jk} - \alpha_{ik}). \tag{18}$$

Applying the chain rule,

$$\frac{\partial L}{\partial s_{ik}} = \sum_{j=1}^{T} \frac{\partial L}{\partial \alpha_{ij}} \frac{\partial \alpha_{ij}}{\partial s_{ik}} \tag{19}$$

$$= \sum_{j=1}^{T} b_{ij}\alpha_{ij}(\delta_{jk} - \alpha_{ik}) \tag{20}$$

$$= \alpha_{ik}b_{ik} - \alpha_{ik}\sum_{j=1}^{T} \alpha_{ij}b_{ij} \tag{21}$$

$$= \alpha_{ik}(b_{ik} - \mathbb{E}_{\alpha_i}[b]). \tag{22}$$

Hence

$$\boxed{\frac{\partial L}{\partial s_{ik}} = \alpha_{ik}\left(b_{ik} - \mathbb{E}_{\alpha_i}[b]\right).} \tag{23}$$

It is convenient to define an *advantage* quantity with the sign chosen to align with gradient descent:

$$A_{ij} := -\left(b_{ij} - \mathbb{E}_{\alpha_i}[b]\right).$$

Under this definition, $A_{ij} > 0$ indicates that increasing s_{ij} (and hence α_{ij}) would reduce the loss. Gradient descent therefore increases attention scores toward positions with positive advantage and decreases them otherwise.

This is an *advantage*-style gradient: scores increase for positions whose compatibility exceeds the current attention-weighted average, and decrease otherwise.

3.5 Gradients to q_i and k_j

We next propagate through the score definition $s_{ij} = q_i^\top k_j / \sqrt{d_k}$.

For fixed i,

$$\frac{\partial L}{\partial q_i} = \sum_{k=1}^{T} \frac{\partial L}{\partial s_{ik}} \frac{\partial s_{ik}}{\partial q_i} = \sum_{k=1}^{T} \frac{\partial L}{\partial s_{ik}} \frac{k_k}{\sqrt{d_k}} \tag{24}$$

$$= \frac{1}{\sqrt{d_k}} \sum_{k=1}^{T} \alpha_{ik}(b_{ik} - \mathbb{E}_{\alpha_i}[b])k_k. \tag{25}$$

Similarly, for fixed j,

$$\frac{\partial L}{\partial k_j} = \sum_{i=1}^{T} \frac{\partial L}{\partial s_{ij}} \frac{\partial s_{ij}}{\partial k_j} = \sum_{i=1}^{T} \frac{\partial L}{\partial s_{ij}} \frac{q_i}{\sqrt{d_k}} \tag{26}$$

$$= \frac{1}{\sqrt{d_k}} \sum_{i=1}^{T} \alpha_{ij}(b_{ij} - \mathbb{E}_{\alpha_i}[b])q_i. \tag{27}$$

Thus,

$$\boxed{\begin{aligned} \frac{\partial L}{\partial q_i} &= \frac{1}{\sqrt{d_k}} \sum_{k=1}^{T} \alpha_{ik}(b_{ik} - \mathbb{E}_{\alpha_i}[b])k_k, \\ \frac{\partial L}{\partial k_j} &= \frac{1}{\sqrt{d_k}} \sum_{i=1}^{T} \alpha_{ij}(b_{ij} - \mathbb{E}_{\alpha_i}[b])q_i. \end{aligned}} \tag{28}$$

Finally, gradients propagate to W_Q and W_K as

$$\nabla_{W_Q} L = \sum_{i=1}^{T} \left(\frac{\partial L}{\partial q_i} \right) x_i^\top, \tag{29}$$

$$\nabla_{W_K} L = \sum_{j=1}^{T} \left(\frac{\partial L}{\partial k_j} \right) x_j^\top. \tag{30}$$

3.6 Gradient to W_V

From $\partial L / \partial v_j = \sum_i \alpha_{ij} u_i$ and $v_j = W_V x_j$,

$$\frac{\partial L}{\partial W_V} = \sum_{j=1}^{T} \left(\frac{\partial L}{\partial v_j} \right) x_j^\top = \sum_{j=1}^{T} \left(\sum_{i=1}^{T} \alpha_{ij} u_i \right) x_j^\top. \tag{31}$$

Letting $U = [u_1, \ldots, u_T] \in \mathbb{R}^{d_v \times T}$, $A = (\alpha_{ij}) \in \mathbb{R}^{T \times T}$, and $X = [x_1, \ldots, x_T] \in \mathbb{R}^{d_x \times T}$, we can write

$$\boxed{\nabla_{W_V} L = U A X^\top.} \tag{32}$$

3.7 First-Order Parameter Updates

For learning rate $\eta > 0$, gradient descent gives

$$\Delta v_j = -\eta \frac{\partial L}{\partial v_j} = -\eta \sum_{i=1}^{T} \alpha_{ij} u_i, \tag{33}$$

$$\Delta s_{ik} = -\eta \frac{\partial L}{\partial s_{ik}} = -\eta \alpha_{ik} \left(b_{ik} - \mathbb{E}_{\alpha_i}[b] \right), \tag{34}$$

$$\Delta q_i = -\eta \frac{\partial L}{\partial q_i}, \tag{35}$$

$$\Delta k_j = -\eta \frac{\partial L}{\partial k_j}. \tag{36}$$

The remainder of the paper analyzes the coupled dynamics induced by these updates.

4 Coupled Dynamics and Specialization

We now unpack the implications of the gradient flows in Section Section 3, focusing on the interaction between routing (via scores and attention) and content (via values).

4.1 Advantage-Based Attention Reallocation

Equation (23) shows that for fixed query i, It is convenient to define an *advantage* quantity with the sign chosen to align with gradient descent:

$$A_{ij} := -\left(b_{ij} - \mathbb{E}_{\alpha_i}[b] \right).$$

Under this definition, $A_{ij} > 0$ indicates that increasing s_{ij} (and hence α_{ij}) would reduce the loss. Gradient descent therefore increases attention scores toward positions with positive advantage and decreases them otherwise.

Thus attention reallocates mass away from positions whose values are worse-than-average (i.e., $b_{ik} > \mathbb{E}_{\alpha_i}[b]$) for u_i and toward those that are better-than-average, implementing an advantage-based routing rule.

4.2 Value Updates as Responsibility-Weighted Prototypes

Define the attention-weighted upstream signal for column j:

$$\bar{u}_j := \sum_{i=1}^{T} \alpha_{ij} u_i. \tag{37}$$

From (33),

$$\Delta v_j = -\eta \bar{u}_j, \tag{38}$$

so v_j moves in the direction that jointly benefits all queries that attend to it, weighted by their attention.

In particular, if a small set of queries uses j heavily, v_j becomes a prototype that serves that subset. This is the core specialization mechanism: values adapt to the error landscape created by their users.

4.3 First-Order Effect on Contexts and Loss

Since $g_i = \sum_k \alpha_{ik} v_k$, an infinitesimal change in v_j induces

$$\Delta g_i = \alpha_{ij} \Delta v_j = -\eta \alpha_{ij} \sum_{r=1}^{T} \alpha_{rj} u_r. \tag{39}$$

Using $u_i = \partial L / \partial g_i$, the first-order change in loss from this perturbation is

$$\Delta L_i \approx u_i^\top \Delta g_i \tag{40}$$

$$= -\eta \alpha_{ij} \sum_{r=1}^{T} \alpha_{rj} (u_i^\top u_r). \tag{41}$$

Interpretation. The factor α_{ij} says: the more query i relies on value j, the more v_j's update affects g_i. The column weights $\{\alpha_{rj}\}$ aggregate contributions from all queries that share j. The inner products $u_i^\top u_r$ measure whether their error directions are aligned (helpful) or opposed (conflicting).

If many u_r align with u_i, then v_j can move in a direction that helps them all. If some are anti-aligned, v_j must compromise, and specialization may become harder.

Dominant-query approximation. If query i is the primary user of key j (i.e., $\alpha_{ij} \gg \alpha_{rj}$ for $r \neq i$), then $\sum_r \alpha_{rj} u_r \approx \alpha_{ij} u_i$ and

$$\Delta g_i \approx -\eta \alpha_{ij}^2 u_i, \tag{42}$$

$$\Delta L_i \approx -\eta \alpha_{ij}^2 \|u_i\|^2 \leq 0. \tag{43}$$

Thus, under this approximation, the update decreases loss for query i by an amount proportional to $\alpha_{ij}^2 \|u_i\|^2$: the stronger the attention and the larger the error, the bigger the immediate improvement.

4.4 Feedback Loop and Specialization

Equations (23) and (33) together form a feedback loop:

(1) If v_j is particularly helpful to i (large negative $b_{ij} - \mathbb{E}_{\alpha_i}[b]$), then s_{ij} increases and α_{ij} grows.
(2) Larger α_{ij} gives u_i more weight in $\bar{u}_j$, so v_j moves further toward u_i.
(3) As v_j aligns with u_i, $b_{ij} = u_i^\top v_j$ increases, reinforcing step 1.

Repeated application yields specialized value vectors that serve distinct subsets of queries, while attention concentrates on these specialized prototypes.
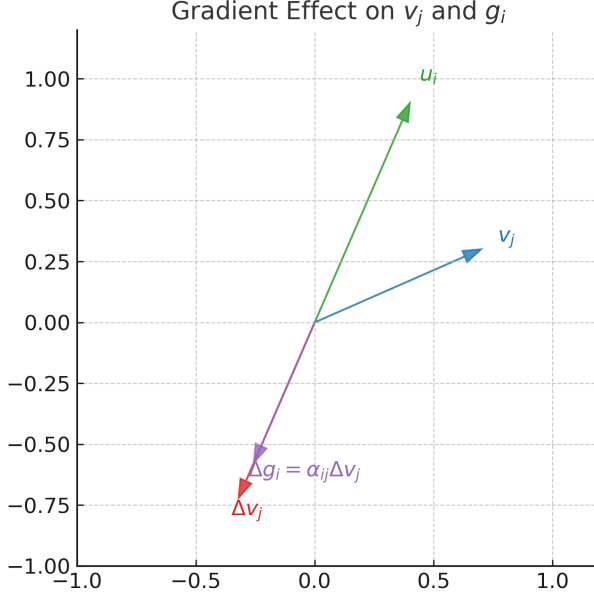
Fig. 1. Geometric illustration of coupled gradient dynamics. Value vector v_j (blue) is updated toward the attention-weighted upstream signal $\bar{u}_j$ (green), inducing a change $\Delta g_i = \alpha_{ij}\Delta v_j$ (purple) in the context for any query i attending to j. This change reduces loss to first order and increases compatibility b_{ij}, which in turn reinforces routing through j.

4.5 Geometric Illustration

Figure Figure 1 schematically illustrates the coupled dynamics: v_j is pulled toward upstream gradient u_i, inducing a change in g_i along a direction that reduces loss; the improved alignment feeds back into the score gradients.

5 EM-Like Two-Timescale Dynamics

The coupled dynamics derived above admit a useful analogy to Expectation–Maximization (EM), not as a literal optimization of an explicit latent-variable likelihood, but as a *mechanistic correspondence* between gradient flows and responsibility-weighted updates. Attention weights behave like soft responsibilities over latent sources, while value vectors act as prototypes updated under those responsibilities. Unlike classical EM, the updates here are driven by upstream gradients rather than observed data, and no standalone likelihood over values is optimized.

5.1 Attention as Responsibilities

For a fixed query i, the attention weights can be viewed as the posterior responsibilities of a latent variable Z_i indicating which source position j is active:

$$\alpha_{ij} = p(Z_i = j \mid q_i, K; \theta) = \frac{\exp(q_i^\top k_j/\sqrt{d_k})}{\sum_k \exp(q_i^\top k_k/\sqrt{d_k})}. \tag{44}$$

The score gradient

$$\Delta s_{ij} \propto -\alpha_{ij}\big(b_{ij} - \mathbb{E}_{\alpha_i}[b]\big)$$

increases responsibilities for positions whose compatibility b_{ij} exceeds the current mean, just as the E-step in EM increases responsibilities for mixture components that explain the data well.

5.2 Values as Prototype Updates

Given responsibilities α_{ij}, the value update

$$v_j^{\text{new}} = v_j^{\text{old}} - \eta \sum_i \alpha_{ij} u_i$$

aggregates feedback from all assigned queries, weighted by their responsibilities. This is directly analogous to the M-step update for cluster means in Gaussian mixture models:

$$\mu_j^{\text{new}} \leftarrow \frac{\sum_i \gamma_{ij} x_i}{\sum_i \gamma_{ij}},$$

with u_i playing the role of residuals that need to be explained.

A key difference from classical mixture-model EM is the role played by u_i. In standard EM, centroids are updated using observed data points. Here, u_i represents the residual error signal backpropagated from the loss. Values therefore move to better explain the *error geometry* induced by the current routing structure, rather than to maximize a likelihood over inputs. The analogy is structural rather than variational.

5.3 Approximate EM vs. SGD

In classical EM, the E-step and M-step are separated: responsibilities are recomputed holding parameters fixed, then parameters are updated holding responsibilities fixed. In transformers trained with SGD, these steps are interleaved and noisy, but the first-order picture still resembles EM:

- **Fast E-step:** Score gradients quickly adjust q_i and k_j so that attention patterns allocate responsibility to helpful positions. In practice, attention often stabilizes early.
- **Slow M-step:** Value vectors continue to move under residual error signals, refining the content manifold even after attention appears frozen. This continues until calibration and likelihood converge.

We can make this connection more explicit by considering a "manual EM" algorithm that alternates:

(1) *E-like step:* Forward pass to compute α_{ij} using current q_i, k_j.
(2) *M-like step on values:* Update v_j with a closed-form gradient step using $\Delta v_j = -\eta \sum_i \alpha_{ij} u_i$ while freezing q_i, k_j.
(3) *Small SGD step on* W_Q, W_K, W_O: Update the nonlinear projection parameters with a small gradient step.

In Section Section 7.2, we compare such an EM-like schedule to standard SGD on a sticky Markov-chain task and find that both converge to similar solutions, but the EM-like updates reach low loss and sharp, focused attention much faster.

5.4 Analogy Table

EM Concept	Attention Equivalent
Latent assignment Z_i	Source index j
Responsibilities γ_{ij}	Attention weights α_{ij}
E-step	Forward pass + score update (23)
Mixture means / centroids	Value vectors v_j
M-step for means	$v_j \leftarrow v_j - \eta \sum_i \alpha_{ij} u_i$
Convergence criterion	Cross-entropy loss, calibration, entropy

5.5 Bayesian vs. EM Perspective

EM is an optimization procedure: it produces a point estimate θ^* maximizing (posterior) likelihood. A fully Bayesian treatment would instead integrate over θ, but is intractable for transformers. Our analysis therefore lives at the EM/SGD level.

Crucially, however, our companion work [1] shows that the point-estimate parameters learned in this way support *Bayesian computation in representation space*: value manifolds, key frames, and query trajectories implement Bayesian belief updates in context. The present paper explains why cross-entropy and gradient descent naturally create these structures.

6 From Gradient Flow to Bayesian Manifolds

We now connect the gradient dynamics derived above to the geometric structures observed in Bayesian wind tunnels and production models.

6.1 Value Manifold Unfurling

In wind-tunnel experiments [1], we observe that:

- Early in training, attention entropy decreases and attention focuses on relevant hypotheses.
- Later in training, attention patterns appear stable, but value representations unfurl along a smooth curve; the first few principal components explain most variance, and the main axis correlates strongly with posterior entropy.
- Calibration error continues to drop even as attention maps remain visually unchanged.

Once score gradients have largely equalized compatibility ($b_{ij} \approx \mathbb{E}_{\alpha_i}[b]$), $\partial L/\partial s_{ij} \approx 0$ and attention freezes. But unless loss is exactly zero, u_i remains non-zero and value updates

$$\Delta v_j = -\eta \sum_i \alpha_{ij} u_i$$

continue, gradually aligning v_j along the principal directions of the residual error landscape. Under repeated updates, values come to lie on low-dimensional manifolds parameterized by downstream functionals such as posterior entropy.

6.2 Hypothesis Frames and Key Orthogonality

The gradients to k_j show that keys are shaped by advantage signals:

$$\frac{\partial L}{\partial k_j} \propto \sum_i \alpha_{ij} \big(b_{ij} - \mathbb{E}_{\alpha_i}[b] \big) q_i.$$

If different subsets of queries consistently find different keys helpful, the corresponding gradient contributions push keys apart in k-space, encouraging approximate orthogonality of distinct

hypothesis axes. Our wind-tunnel paper measures exactly this orthogonality and connects it to clean separation of competing hypotheses.

6.3 Frame–Precision Dissociation

The empirically observed *frame–precision dissociation*—attention stably defining a hypothesis frame while calibration continues to improve—is now easy to interpret:

- The *frame* is defined by q_i, k_j and attention weights α_{ij}. This stabilizes when advantage signals equalize and $\partial L/\partial s_{ij} \approx 0$.
- *Precision* lives in the arrangement of values v_j along manifolds that support fine-grained likelihood modeling. This continues to refine as long as u_i is non-zero.

Thus, a late-stage transformer has a fixed Bayesian frame (hypothesis axes and routing) but continues to sharpen its posterior geometry.

7 Experiments

We now illustrate the theory with controlled simulations. All experiments use a single-head, single-layer attention block without residual connections or LayerNorm to keep the dynamics transparent.

7.1 Toy Attention Simulation

We first consider a small toy setup with $T = 5$, $d_x = 3$, $d_k = 2$, $d_v = 2$, and $C = 3$ classes.

Setup.

- Projection matrices W_Q, W_K, W_V, W_O are initialized with small Gaussian entries.
- Inputs x_j are drawn from $\mathcal{N}(0, I)$.
- Targets y_i are random in $\{0, 1, 2\}$.
- We run manual update steps using the closed-form gradients from Section Section 3, with a fixed learning rate.

Observations. Over ~ 100 steps we observe:

(1) Attention heatmaps sharpen: mass concentrates on a few positions per query (Figures Figure 2, Figure 3).
(2) Value vectors move coherently in a low-dimensional subspace; their trajectories in a PCA projection show emergent manifold structure (Figure Figure 5).
(3) Cross-entropy loss decays smoothly (Figure Figure 4), with most gains occurring as specialization emerges.

7.2 Sticky Markov-Chain Simulation: EM vs. SGD

We next study a more structured task where attention can exploit temporal persistence: a sticky Markov chain over symbols.

Task. We generate sequences of length $T = 2000$ over an 8-symbol vocabulary $\{0, \ldots, 7\}$ from a first-order Markov chain with self-transition probability $P(y_{t+1} = y_t \mid y_t) = 0.3$, otherwise transition to a different state with probability proportional to modulo distance of 7 with probability proportional to the distance from the previous state. With this circular distance, the nearby symbol gets higher probability than the distant one. Each symbol y_t has an associated mean embedding in $\mathbb{R}^{20}$; the input at time t is $x_t = \mu_{y_{t-1}} + \epsilon_t$ with $\epsilon_t \sim \mathcal{N}(0, I)$, so embeddings carry information about the previous symbol.
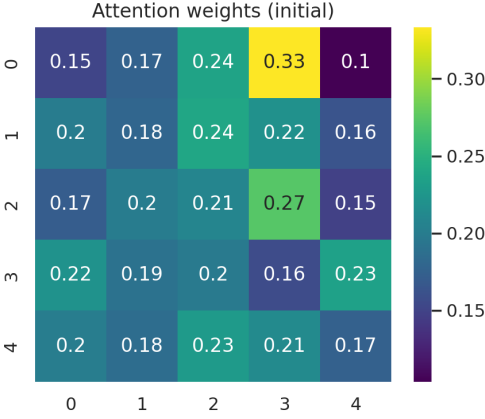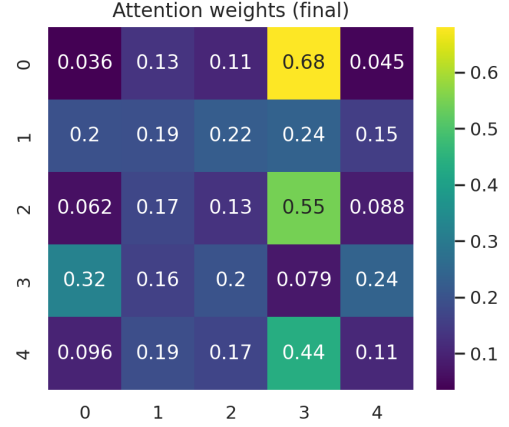
Fig. 2. Initial attention heatmap (toy simulation)

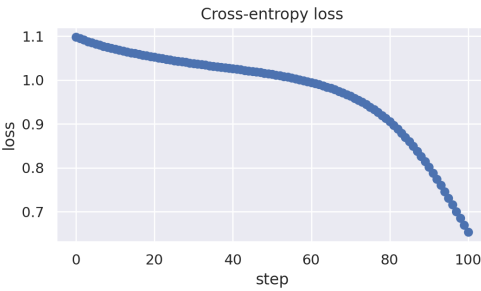Fig. 3. Final attention heatmap, 100 steps (toy simulation)
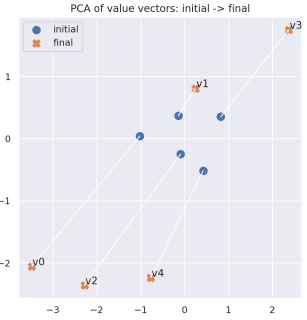

Fig. 4. Loss, 100 EM steps (toy simulation)

Fig. 5. PCA projection of value vectors v_j (toy simulation)

We train a single-head attention layer with $d_x = 20$, $d_k = d_q = 10$, $d_v = 15$ for 1000 steps to predict y_t from $(x_1, \ldots, x_t)$.

Protocols. We compare two training schemes with causal masking:

(1) **Standard SGD.** Vanilla gradient descent on all parameters with a fixed learning rate.
(2) **EM-like schedule.** Alternating steps:
   - E-like step: forward pass to compute α_{ij} and u_i.
   - M-like step: update v_j using the closed-form gradient $\Delta v_j = -\eta \sum_i \alpha_{ij} u_i$.
   - Small SGD step on W_Q, W_K, W_O to adjust the latent assignment model.

Metrics. We track:

- final cross-entropy loss,
- final accuracy,
- predictive entropy,
- KL(EM ∥ SGD) of the predictive distributions.

Results. Table Table 1 summarizes the results after a fixed budget of steps.

Table 1. Sticky Markov-chain task: EM-like vs. standard SGD with stay_prob=0.3, after 1000 steps. EM achieves lower loss, higher accuracy, and sharper (lower entropy) predictive distributions. The theoretical Bayesian minimum predictive entropy is computed assuming $x_{t+1} = y(t)$. True theoretical predictive entropy would be slightly higher, since $x_t = y_{t-1} + \epsilon_t$, $\epsilon_t \sim \mathcal{N}_{d_x}(0, I)$, which increases entropy. The increase is small by the central limit theorem, since the noise $\mathcal{N}(0, I)$ is averaged over d_x dimensions. The final row reports the KL divergence between EM and SGD predictive distributions.

Metric	Value
final_loss_EM	1.8961
final_loss_sgd	1.9177
final_acc_EM	0.2690
final_acc_sgd	0.2675
final_entropy_EM	1.9076
final_entropy_sgd	1.9276
Theoretical Min entropy	1.8833
final_KL(EM|SGD)	0.1019

Figures Figure 6–Figure 8 plot loss, accuracy, and entropy as a function of training step. As expected, EM and SGD methods converge to the same solution. This may not always happen due to local minima. EM converges much faster, with loss and entropy dropping sharply and accuracy rising quickly, while SGD progresses more slowly. This happens since v_j are optimized directly in the function space, unlike SGD which optimizes in the parameter space. The argument is similar to functional gradient boost that converges faster than parameter updates (@[4]). It is also interesting to note that even with this single layer and head architecture, the final empirical predictive entropy is very close to the theoretically minimum Bayesian entropy as described in Table 1. The theoretical entropy is higher due to addition of noise in defining x_{t+1}.
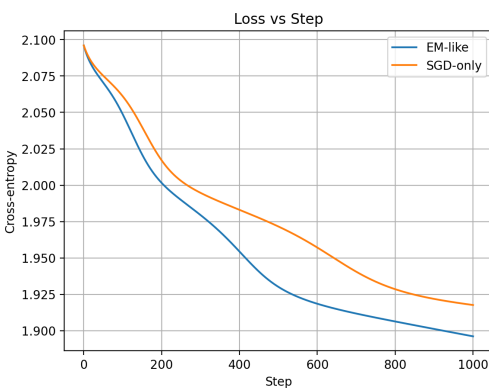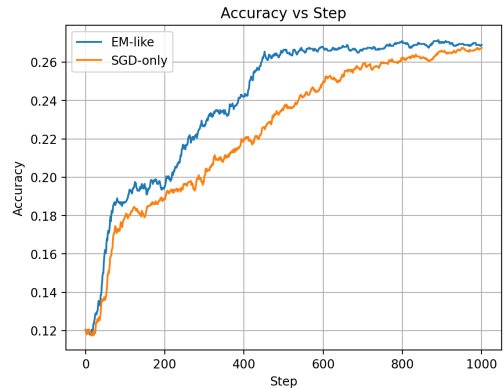

Fig. 6. Sticky Markov Chain: Loss Dynamics

Fig. 7. Sticky Markov Chain: Accuracy Dynamics

To compare micro behavior of EM and sgd, we computed the movement of v vector for EM and sgd. Since $T = 2000$, we will have 2000 v_j for each, EM and sgd. For clearer visualization we show a sample of 200 $v's$. The PCA projection plot of these 200 v_j vectors trajectories is quite insightful. It shows (Figure Figure 9) that EM induces longer, more coherent trajectories from initial to final positions than SGD, consistent with stronger, more focused specialization. Red arrows (SGD) are
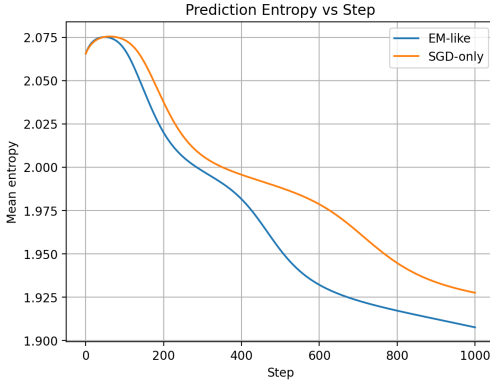
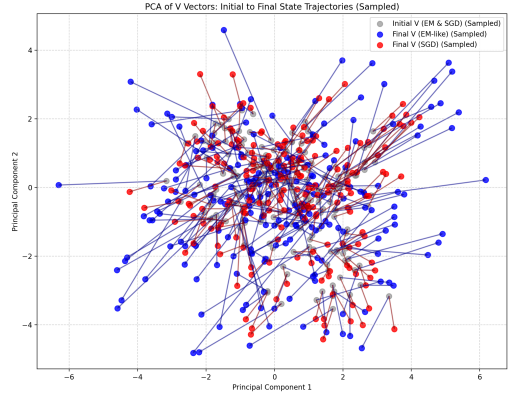Fig. 8. Sticky Markov Chain: Prediction Entropy

Fig. 9. Sticky Markov Chain: 200 Sampled PCA of V

shorter and more scattered; blue arrows (EM) are longer and more aligned, indicating that the EM-like updates exploit the analytic form of the value gradient more effectively.

Takeaways. Both EM-like and SGD training ultimately converge toward similar qualitative solutions: specialized values and focused attention. However, the EM-like schedule reaches this state with fewer steps and sharper specialization. This matches the two-timescale story: responsibilities (attention) can be treated as approximately converged, and closed-form value updates can exploit this stability to accelerate manifold formation.

8 Practical Implications and Diagnostics

The gradient analysis suggests useful diagnostics and design principles for training and interpreting transformer attention.

8.1 Diagnostics

- **Compatibility matrix** $B = (b_{ij})$. Monitoring $b_{ij} = u_i^\top v_j$ reveals which values are most helpful to which queries.
- **Advantage matrix** $A^{\mathbf{adv}} = (b_{ij} - \mathbb{E}_{\alpha_i}[b])$. The sign and magnitude predict where attention will strengthen or weaken.
- **Column usage** $\sum_i \alpha_{ij}$. Low column sums identify underused or dead values.
- **Value norms** $\|v_j\|$. Norm trajectories can flag potential instability (exploding or vanishing norms).

8.2 Regularization and Stability

- **LayerNorm on values** can stabilize norms while leaving directional dynamics intact.
- **Attention dropout** disrupts the feedback loop, limiting over-specialization and encouraging more evenly used values.
- **Learning rate choices** modulate the timescale separation between routing and content; smaller learning rates make the first-order picture more accurate.

8.3 Architectural Choices

- **Multi-head attention** allows multiple specialized routing manifolds, reducing competition within a single head.

- **Depth** naturally supports the binding–elimination–refinement hierarchy observed in our wind-tunnel experiments and large models.
- **Residual connections** help maintain useful intermediate representations even as individual heads specialize strongly.

9 Related Work

9.1 Bayesian Interpretations of Transformers

Several works argue that transformers implement approximate Bayesian inference, either behaviorally or via probing [e.g. 7, 8]. Our companion paper [1] demonstrates exact Bayesian behavior and geometric signatures in small wind tunnels, while a scaling paper shows similar patterns in production LLMs. The present work explains *how* gradient dynamics produce these geometries. It further shows that minimum theoretical Bayesian predictive entropy is close to the empirical entropy. This is studied in greater detail in the companion paper.

9.2 Mechanistic Interpretability

Mechanistic interpretability studies identify specific heads and circuits performing copy, induction, and other algorithmic tasks [3, 5]. Our framework complements this line by explaining how specialization arises from the interaction between routing and content, rather than treating specialized heads as primitive.

9.3 Optimization and Implicit Bias

The implicit bias of gradient descent in linear and deep networks has been extensively studied [2, 6]. We extend these ideas to attention: gradient descent implicitly favors representations where routing aligns with error geometry and values lie on low-dimensional manifolds that support Bayesian updating.

The responsibility-weighted value updates derived here are reminiscent of neural EM and slot-attention models, where soft assignments drive prototype updates. The key distinction is that, in transformers, responsibilities are computed via content-addressable attention and prototype updates are driven by backpropagated error signals rather than reconstruction likelihoods. Our focus is not on proposing a new EM-style architecture, but on showing how standard cross-entropy training in attention layers induces EM-like specialization dynamics as a consequence of gradient flow.

10 Limitations and Future Directions

Our analysis is deliberately minimal and controlled.

First-order approximation. We work in a first-order regime, assuming small learning rates and ignoring higher-order and stochastic effects (e.g., momentum, Adam, mini-batch noise). Extending the analysis to realistic optimizers is an important next step.

Single-head, single-layer focus. We analyze a single head in isolation, without residual pathways or LayerNorm. Multi-head, multi-layer dynamics—including inter-head coordination and hierarchical specialization—remain open.

Finite vs. infinite width. We do not explicitly connect our analysis to the neural tangent kernel or infinite-width limits. Bridging these regimes may help clarify when transformers operate in a feature-learning versus lazy-training mode.

Large-scale empirical validation. Our toy simulations are intentionally small. Applying the diagnostics in Section Section 8 to full-scale LLM training runs, tracking advantage matrices and manifold formation over time, is a promising direction.

11 Conclusion

This paper focuses on first-order mechanisms in a minimal setting; companion work establishes that the same geometric structures persist at scale and support exact Bayesian inference in controlled wind tunnels and large models.

Our key findings are:

(1) **Advantage-based routing.** Score gradients $\partial L/\partial s_{ij} = \alpha_{ij}(b_{ij} - \mathbb{E}_{\alpha_i}[b])$ implement an advantage rule that reallocates attention toward above-average values.

(2) **Responsibility-weighted value updates.** Values evolve via $\Delta v_j = -\eta \sum_i \alpha_{ij} u_i$, becoming prototypes for the queries that attend to them.

(3) **Coupled specialization.** Routing and content form a positive feedback loop that produces specialized values and focused attention.

(4) **Two-timescale EM behavior.** Attention often stabilizes early (E-step), while values refine more slowly (M-step), explaining the observed frame–precision dissociation.

(5) **Manifold formation.** The same gradient dynamics that reduce cross-entropy loss also sculpt the low-dimensional manifolds that implement Bayesian posteriors in representation space.

Together with our wind-tunnel and scaling papers, this yields a coherent trilogy: optimization dynamics construct Bayesian geometry, and that geometry enables transformers to behave as Bayesian reasoners in context.

References

[1] Naman Agarwal, Siddhartha R. Dalal, and Vishal Misra. 2025. The Bayesian Geometry of Transformer Attention. arXiv:2512.22471 [cs.LG] https://arxiv.org/abs/2512.22471 Paper I of the Bayesian Attention Trilogy.

[2] Jimmy Ba, Murat A Erdogdu, Marzyeh Ghassemi, Taiji Suzuki, Denny Wu, and Tianzong Zhang. 2022. High-dimensional asymptotics of feature learning: How one gradient step improves the representation. *Advances in Neural Information Processing Systems* 35 (2022).

[3] Nelson Elhage, Neel Nanda, Catherine Olsson, Tom Henighan, Nicholas Joseph, Ben Mann, Amanda Askell, Yuntao Bai, Anna Chen, Tom Conerly, Nova DasSarma, Dawn Drain, Deep Ganguli, Zac Hatfield-Dodds, Danny Hernandez, Andy Jones, Jackson Kernion, Liane Lovitt, Kamal Ndousse, Dario Amodei, Tom Brown, Jack Clark, Jared Kaplan, Sam McCandlish, and Chris Olah. 2021. A Mathematical Framework for Transformer Circuits. Transformer Circuits Thread, Anthropic. https://transformer-circuits.pub/2021/framework/index.html

[4] Jerome H. Friedman. 2001. Greedy Function Approximation: A Gradient Boosting Machine. *The Annals of Statistics* 29, 5 (2001), 1189–1232.

[5] Catherine Olsson, Nelson Elhage, Neel Nanda, Nicholas Joseph, Nova DasSarma, Tom Henighan, Ben Mann, Amanda Askell, Yuntao Bai, Anna Chen, Tom Conerly, Dawn Drain, Deep Ganguli, Zac Hatfield-Dodds, Danny Hernandez, et al. 2022. In-Context Learning and Induction Heads. Transformer Circuits Thread, Anthropic. https://transformer-circuits.pub/2022/in-context-learning-and-induction-heads/index.html

[6] Daniel Soudry, Elad Hoffer, Mor Shpigel Nacson, Suriya Gunasekar, and Nathan Srebro. 2018. The implicit bias of gradient descent on separable data. *Journal of Machine Learning Research* 19, 70 (2018), 1–57.

[7] Johannes von Oswald, Christian Henning, Adrià Garriga-Alonso, Massimo Caccia, Frederik Träuble, Benjamin F. Grewe, Bernhard Schölkopf, Claudia Clopath, and Johanni Brea. 2023. Transformers as Meta-Learners for Bayesian Inference. *arXiv preprint arXiv:2305.14034* (2023).

[8] Sang Michael Xie, Aditi Raghunathan, Percy Liang, and Tengyu Ma. 2022. An Explanation of In-Context Learning as Implicit Bayesian Inference. In *International Conference on Learning Representations*.